

## Research Article

# Analysis of SO<sub>2</sub> Pollution Changes of Beijing-Tianjin-Hebei Region over China Based on OMI Observations from 2006 to 2017

Zhifang Wang,<sup>1,2</sup> Fengjie Zheng<sup>1</sup> ,<sup>1</sup> Wenhao Zhang,<sup>1</sup> and Shutao Wang<sup>2</sup>

<sup>1</sup>*Institute of Remote Sensing and Digital Earth, Chinese Academy of Sciences, Beijing 100101, China*

<sup>2</sup>*Department of Instrument Science & Engineering, Yanshan University, Qinhuangdao, Hebei 066004, China*

Correspondence should be addressed to Fengjie Zheng; zhengfj@radi.ac.cn

Received 22 February 2018; Accepted 6 June 2018; Published 16 July 2018

Academic Editor: Pedro Salvador

Copyright © 2018 Zhifang Wang et al. This is an open access article distributed under the Creative Commons Attribution License, which permits unrestricted use, distribution, and reproduction in any medium, provided the original work is properly cited.

Sulfur dioxide (SO<sub>2</sub>) in the planetary boundary layer (PBL) as a kind of gaseous pollutant has a strong effect regarding atmospheric environment, air quality, and climate change. As one of the most polluted regions in China, air quality in Beijing-Tianjin-Hebei (BTH) region has attracted more attention. This paper aims to study the characteristics of SO<sub>2</sub> distribution and variation over BTH. Spatial and temporal variations for a long term (2006–2017) over BTH derived from OMI PBL SO<sub>2</sub> products were discussed. The temporal trends confirm that the SO<sub>2</sub> loading falls from average 0.88 DU to 0.16 DU in the past 12 years. Two ascending fluctuations in 2007 and 2011 appeared to be closely related to the economic stimulus of each five-year plan (FYP). The spatial analysis indicates an imbalanced spatial distribution pattern, with higher SO<sub>2</sub> level in the southern BTH and lower in the northern. This is a result of both natural and human factors. Meanwhile, the SO<sub>2</sub> concentration demonstrates a decreasing trend with 14.92%, 28.57%, and 27.43% compared with 2006, during the events of 2008 Olympic Games, 2014 Asia-Pacific Economic Cooperation (APEC) summit, and 2015 Military Parade, respectively. The improvement indicates that the direct effect is attributed to a series of long-term and short-term control measures, which have been implemented by the government. The findings of this study are desirable to assist local policy makers in the BTH for drawing up control strategies regarding the mitigation of environmental pollution in the future.

## 1. Introduction

Sulfur dioxide (SO<sub>2</sub>) is a short-lived gas primarily produced by volcanoes, power plants, refineries, metal smelting, and burning of fossil fuels. When SO<sub>2</sub> remains near the Earth's surface, it is toxic, causes acid rain, and degrades air quality. It forms sulfate aerosols that can alter cloud reflectivity and precipitation in the free troposphere [1, 2]. As a kind of important atmospheric pollutants, SO<sub>2</sub> critically affects the global environment, climate change, and public health. SO<sub>2</sub> has become one of the popular research topics in the past decades, to examine its changes over some of the world's most polluted regions [3–10].

China, with its incredible economic growth has been the focus of many studies during the previous decade because of its increasing sulfur dioxide emissions' contribution to the Earth's atmosphere [11–16]. The sources of SO<sub>2</sub> are both natural (volcanic) and anthropogenic emissions. Natural

emissions include intentional biomass burnings and volcanic eruptions. Anthropogenic emissions are mainly due to fossil fuel burning (e.g., coal and oil), which accounts for more than 75% of global emissions [3]. Anthropogenic SO<sub>2</sub> emissions are predominantly in or slightly above the planetary boundary layer (PBL), impacting on regional variations of aerosol types [17].

Satellite measurements of trace gases have been widely used and been an essential way to provide global, consistent observations for detecting, monitoring, and quantifying the SO<sub>2</sub>. The first space-based quantitative data on SO<sub>2</sub> mass of the El Chichon volcanic eruption in 1983 were obtained from Total Ozone Mapping Spectrometer (TOMS) on board Nimbus 7 [18]. Subsequently, anthropogenic SO<sub>2</sub> sources from power plants in eastern Europe [19, 20] and smelters in Peru and Russia [21] were demonstrated through detection of SO<sub>2</sub> emissions using Global Ozone Monitoring Experiment (GOME) measurements on the Earth Research

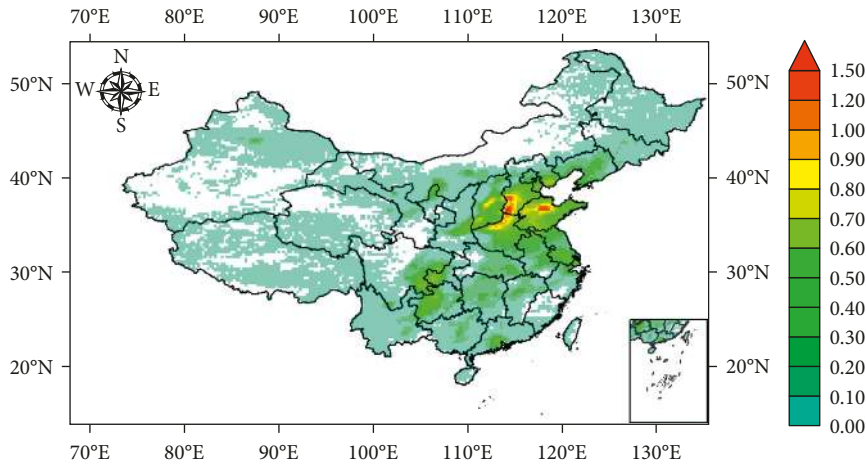


FIGURE 1: The average  $\text{SO}_2$  spatial distribution (in DU) map (2006–2017) over China.

Satellite 2 (ERS-2). The tropospheric  $\text{SO}_2$  were detected by the SCanning Imaging Absorption spectroMeter for Atmospheric CHartography (SCIAMACHY) on board the ENVISAT [22] and the Global Ozone Monitoring Experiment-2 (GOME-2) instrument on MetOp-A [23]. The Ozone Monitoring Instrument (OMI) on NASA's Aura spacecraft enables to provide daily, nearly global measurements of ozone columns and aerosols, and the trace gases with the highest spatial resolution and the longest data record currently available [24, 25].

OMI data have been applied to assess the effect of pollutant transmission, analyze pollutant source contribution, evaluate pollutant emission inventory, observe regional pollution changes, and quantify the reduction of power plant emissions [14, 16, 17, 26–28], due to the higher spatial and temporal resolution. Three major air pollutants ( $\text{NO}_2$ ,  $\text{SO}_2$ , and CO) in China before, during, and after the Olympic Games from Aura's Ozone Monitoring Instrument (OMI) and Terra's Measurements of Pollutants in the Troposphere (MOPITT) instrument have been measured [29]. Annual emissions by sector and fuel types calculated from satellite data show an increasing trend of  $\text{SO}_2$  during 1996–2008 and decreasing thereafter in China [16]. Substantial changes in  $\text{SO}_2$  emissions in the northern China for the period 2005–2008 were analyzed [14]. The spatiotemporal variation of  $\text{SO}_2$  concentration during 2005–2008 over China from the planetary boundary layer (PBL)  $\text{SO}_2$  column concentration retrieved from OMI has been analyzed [28]. Long-term  $\text{SO}_2$  pollution changes over China or region have been observed through OMI observations [29]. A long-term trend of  $\text{NO}_2$  and  $\text{SO}_2$  levels (2005–2014) of the Henan province in China has been retrieved from the OMI [30]. In the past decades, China has adopted different policies for air quality control consistently, such as carbon reduction, energy saving, and other measures to reduce  $\text{SO}_2$  emissions [31, 32]. The latest findings represent that large reductions in  $\text{SO}_2$  are benefiting from the effective control policies in China [33, 34].

In this study, we analyze trend variation and distribution in  $\text{SO}_2$  concentrations over the Beijing-Tianjin-Hebei (BTH) region observed by the OMI between January 2006 and December 2017. Figure 1 shows the multiyear average spatial distribution map of  $\text{SO}_2$  based on OMI data (2006–2017)

over China, which clearly shows the hotspots of  $\text{SO}_2$  in the North China Plain. Meanwhile, it is noted that the BTH region is one of the most polluted regions in China. Accordingly, tight emission control arrangement of this area always adopted, the  $\text{SO}_2$  emission of Hebei rank 3rd in 2013 went down to 5th with 17.4% rate of decline among all provinces in China, and Beijing and Tianjin declined 24.1% and 17.2%, respectively. Regional  $\text{SO}_2$  time evolution and spatial distribution are discussed in the following. The datasets and monitoring area are presented in Section 2. The analysis and associated findings are described in Section 3. Finally, the main conclusions are summarized in Section 4.

## 2. Method Description

**2.1. Data Sources.** Data used in this study over the BTH are based on OMI  $\text{SO}_2$  products with Dobson Units (DU,  $1 \text{ DU} = 2.69 \times 10^{16} \text{ molecules/cm}^2$ ). The Ozone Monitoring Instrument (OMI) is a sun-synchronous polar orbiting Dutch/Finnish sensor on the AURA satellite launched on 15 July 2004. The science goals of OMI are directly related to these questions and focus on (1) measuring the ozone layer and its destroying trace gases BrO and OClO, (2) tropospheric pollution by ozone, nitrogen dioxide, tropospheric aerosols,  $\text{SO}_2$ , and formaldehyde, and (3) detection of species important for climate change such as aerosols, clouds, and ozone. The OMI measures the radiation back-scattered by the Earth's atmosphere and surface over the entire wavelength range from 270 to 500 nm, with a spectral resolution of about 0.5 nm, and high spatial resolution ( $13 \times 24 \text{ km}^2$ ), and daily global coverage [24]. OMI data have 4 processing grade products: Level-0, Level-1, Level-2, and Level-3. For this study, we used the PBL  $\text{SO}_2$  vertical column density from the Level-3  $0.25 \times 0.25$  degree gridded OMI/AURA  $\text{SO}_2$  data product. The data used here with the time span of January 1, 2006 to December 31, 2017, were obtained from Giovanni interface (<http://giovanni.gsfc.nasa.gov/giovanni/>), derived from the NASA Goddard Earth Sciences Data Active Archive Center (GES DISC; <http://disc.sci.gsfc.nasa.gov>) [35, 36]. These Level-3 products have been widely used [15, 34, 37, 38]. The original OMI PBL  $\text{SO}_2$

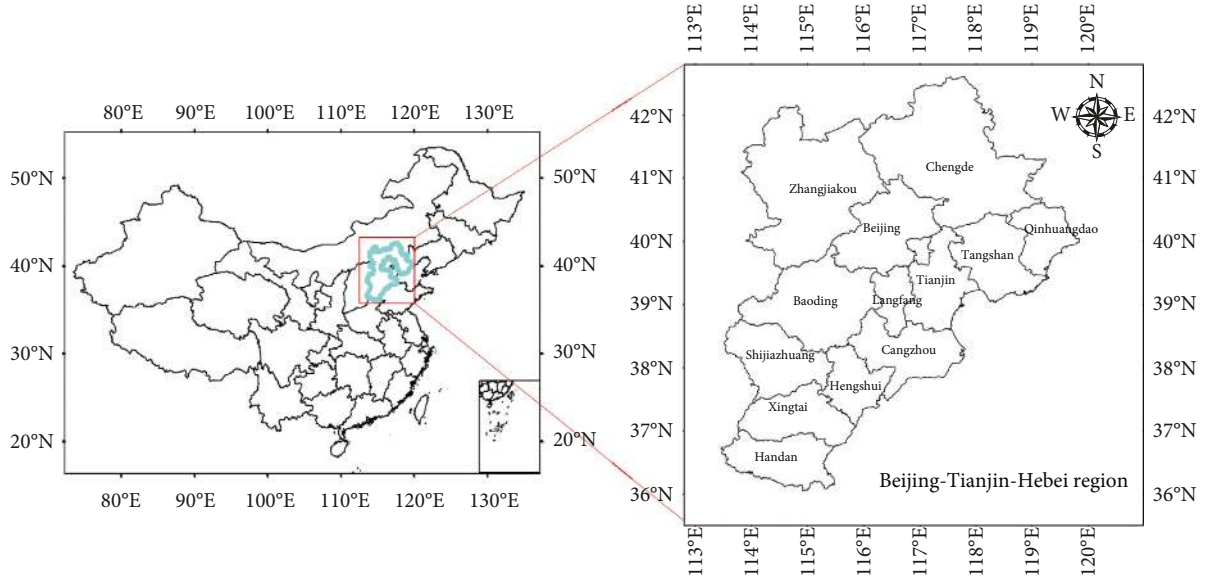


FIGURE 2: Location of the study area in this study. The right image represents the region of Beijing-Tianjin-Hebei.

TABLE 1: Relevant information for study areas (data based on 2016).

Name	Area (km <sup>2</sup> )	Population (10 <sup>4</sup> )	Vehicles (10 <sup>4</sup> )	GDP (10 <sup>9</sup> )	Coal consumption (Mt)
Beijing	1.68	2173	547.44	25669	11.65
Tianjin	1.13	1562	273.69	17885	45.39
Hebei	18.77	7470	1245.89	32070	289.43

product employed the band residual difference (BRD) algorithm [39]. But this product has a high noise level and systematic artifacts that required empirical corrections [5, 6]. A new operational OMI PBL SO<sub>2</sub> product produced with the principal component analysis (PCA) algorithm was released [40, 41]. Validation of these two algorithmic products has been analyzed [42].

Daily satellite observations were retrieved with the given longitude and latitude for China and BTH region, as shown in Figure 2, to gain insight into the distribution of SO<sub>2</sub> columns in the BTH region. The data were gridded onto monthly 0.25 × 0.25 fields and then onto seasonal and yearly maps. The meteorological conditions used for analysis are from NCEP reanalysis data (<https://www.esrl.noaa.gov/psd/>).

**2.2. Study Area.** Our study area focuses on the Beijing-Tianjin-Hebei (BTH) region (Beijing, Tianjin, and Hebei integration), which is the most polluted industrialized regions in China (Figure 1). The BTH region is located in the northwest part of the North China Plain as shown in Figure 2 (36°05′–42°37′N, 113°11′–119°45′E), with a total area of 216,000 km<sup>2</sup> and more than 110 million residential population. The BTH region includes two municipalities (Beijing and Tianjin) and one province (Hebei) (Table 1), which contain thirteen cities: Beijing, Tianjin, Baoding, Langfang, Tangshan, Shijiazhuang, Xingtai, Handan, Cangzhou, Hengshui, Qinhuangdao, Chengde, and Zhangjiakou.

As one of the most economically vibrant regions in China, the BTH region covers only 2.3% of the Chinese

territory but generates over 10% of the total national gross domestic product (GDP) in 2016 (National Bureau of Statistics of China (NBSC)) [43]. As the main high-tech and heavy industry base of China, there are mainly the automotive industry, electronic industry, machinery industry, iron industry, and steel industry. The SO<sub>2</sub> map (Figure 2) shows hotspots associated with the major coal-fired power plants and industrial activities. Figure 3 reveals that high sulfur coal-fired power plants are the major contributors to the SO<sub>2</sub> concentrations over the BTH region [44, 45]. OMI-derived spatial distribution shows generally good agreement with these main anthropogenic emission sources from burning sulfur-contaminated fossil fuels as Figure 3. The last decade has seen frequent occurrences of severe air pollution episodes (haze), and the high SO<sub>2</sub> loading observed certainly contributed to PM 2.5 problems, especially in winter. Atmospheric environment quality has attracted more and more attention related to air pollution prevention and control policy-making.

### 3. Results and Discussion

The temporal and spatial variations of SO<sub>2</sub> concentration in the region of Beijing-Tianjin-Hebei during the period of 2006–2017 were analyzed based on the satellite OMI data to characterize the variation of SO<sub>2</sub> columns.

#### 3.1. Overall Temporal Trend of SO<sub>2</sub>

**3.1.1. SO<sub>2</sub> Decadal Change.** Figure 4(a) clearly shows the annual average SO<sub>2</sub> concentration time series change trend over

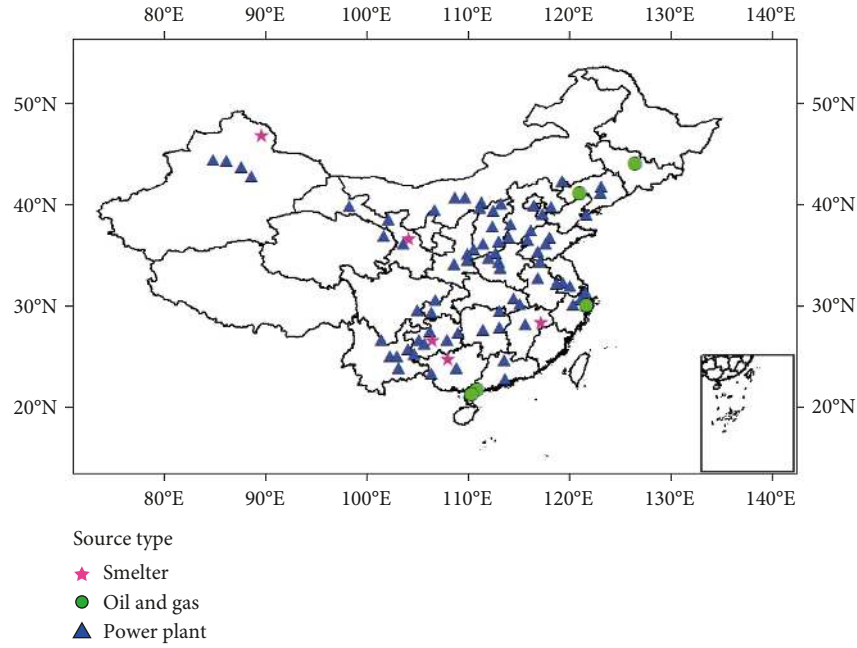


FIGURE 3: Geographic distribution of the major  $\text{SO}_2$  sources in China.

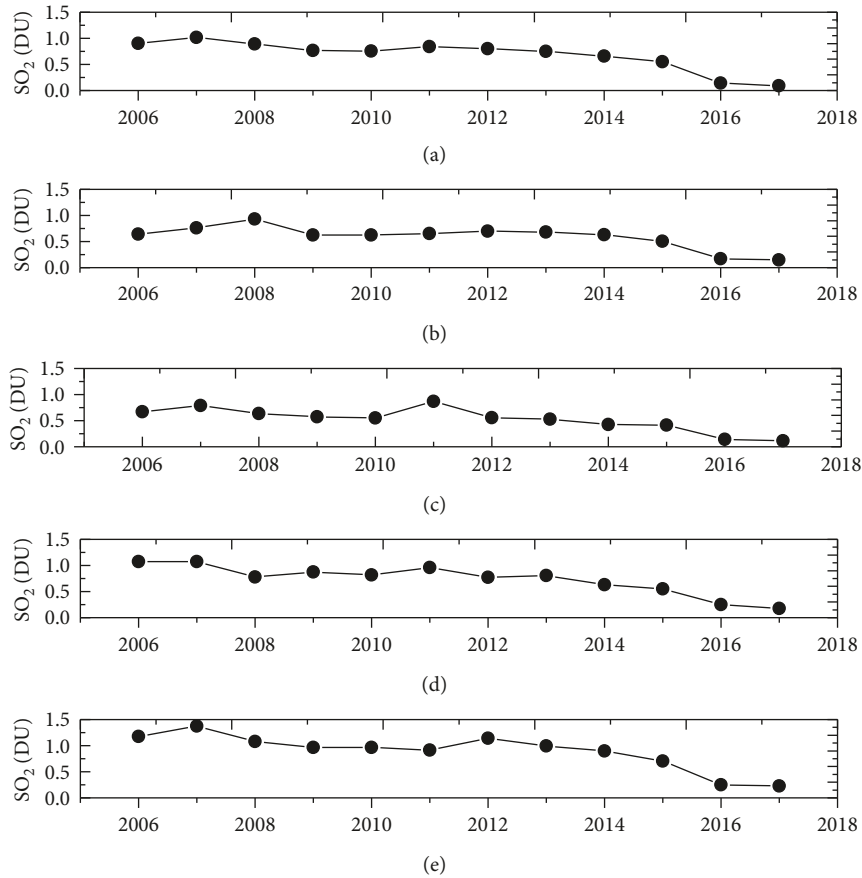


FIGURE 4: Long trend of  $\text{SO}_2$  (DU) over Beijing-Tianjin-Hebei region. (a) Annual average, (b) spring average, (c) summer average, (d) autumn average, and (e) winter average.

BTH from 2006 to 2017. The  $\text{SO}_2$  loading has decreased over the recent years without clear regularity, which is in line with the study results by others [41, 46]. The plot describes the irregular

upward and downward rule. It is necessary to identify the specific period for the pollution attenuation, to a certain extent, related to governmental actions. It was found that  $\text{SO}_2$  peak in

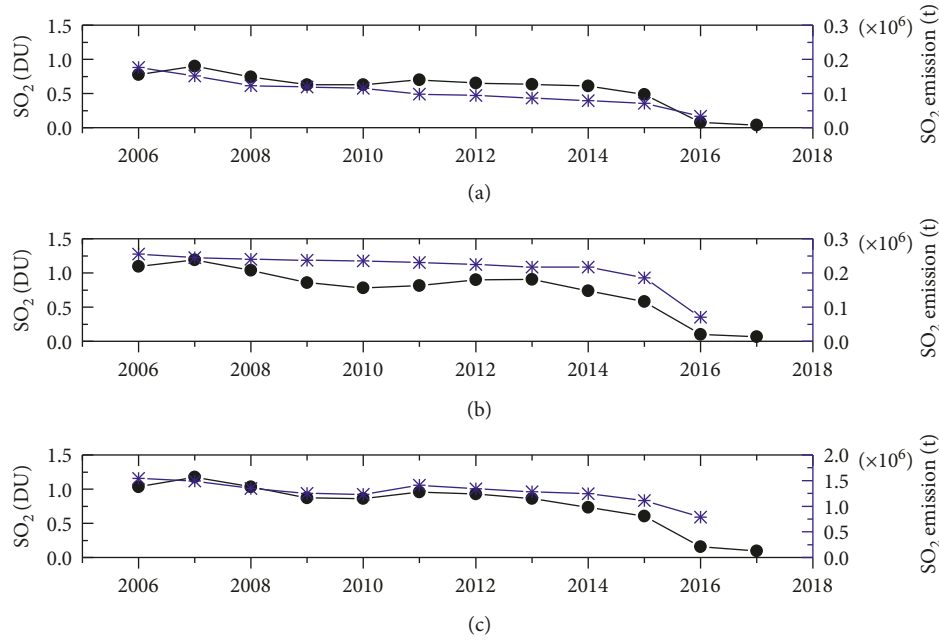


FIGURE 5: Annual average  $\text{SO}_2$  column (DU) based on OMI (black circle dots) and  $\text{SO}_2$  emission statistics (blue asterisks) in (a) Beijing, (b) Tianjin, and (c) Hebei province (statistical data for 2017 have not been published).

2007 with an upward of 14.96% compared to 2006, reflecting the total  $\text{SO}_2$  emission in China had substantially increased from 2000 to 2007. The phenomenon has been largely driven by expansion in manufacturing industries and fueled by coal for the Chinese economic growth [14]. And then, an obvious downward trend appeared from 2007 to 2010, and the decline was 12.92% in 2007–2008 and 13.23% in 2008–2009, respectively. Afterwards from 2009 to 2010, the downward trend slowed down with the rate of decline 0.68%. The decrease was mainly due to China's 11th FYP requiring power plants to install FGD devices.

Nonetheless, there was a temporary rebound from 2010 to 2011 with 19.19% growth rate. The brief period of emission growth can probably be attributed to the government stimulus for resurgence of economy in response to the global financial crisis of 2007–2008. Subsequently, there was a sharp decrease with 37.48% reduction over the 7-year period during 2011–2017. Through the seasonal variation tendency (Figures 4(b)–4(e)), the increase in 2011 mostly comes from summer, accompanied by the industrial production slowdown in the latter half of 2011.

As an industrialized and populated region, the levels of BTH air pollution are determined by population density, economic activity, type of power generation and fuel used, and regulatory policies [47]. Here, we examine the  $\text{SO}_2$  changes with the regional  $\text{SO}_2$  emission data derived from national statistics (<http://www.stats.gov.cn/tjsj/>). It is interesting to find out the yearly emission trend that agrees well with the trend based on OMI retrieved  $\text{SO}_2$  as mentioned earlier (Figure 5), along with the estimated  $\text{SO}_2$  emissions data from power plants. Some mismatch is expected considering the different observation means and uncertainties with satellite and ground measurements.

Two fluctuations occur in the long trends; therefore, we broke down the data into two periods, 2006–2010 and

2011–2017, to verify the coherence with precursors' investigation [30, 48] as to the changes in  $\text{SO}_2$  loadings. Figure 6 shows the 5-year mean  $\text{SO}_2$  concentration distribution maps over the BTH region of China's 11th five-year plan (2006–2010) and second 7 years mean  $\text{SO}_2$  meets China's 12th five-year plan (2011–2015) and China's new 13th five-year plan (2016–2017), respectively. The dramatic decrease in  $\text{SO}_2$  loading (Figure 6) well illustrates the achievements and improvements due to a series of air pollution control policies. The average  $\text{SO}_2$  was 0.87 DU for 2006–2010 (Figure 6(a)). The average concentration decreased to 0.72 DU for 2011–2015 and 0.23 DU for 2016–2017.

According to the above statistics (Figure 5), it is more clearly shown that the  $\text{SO}_2$  loading over the BTH peaked in 2007, and then presented overall decreasing trend. This can be attributed to the emission control measures taken by the government. The sharp decline from 2007 to 2010 is closely related to the installation of flue gas desulfurization (FGD) and follow-up effects of strict pollution reduction measures implemented before the 2008 Beijing Olympic Games. The results also show that atmospheric  $\text{SO}_2$  loadings in BTH have drastically decreased by 17.24% (2011–2015) and 75.29% (2016–2017) related to the average quantity in 11th five-year plan (2006–2010), due to more stricter emission reduction targets, such as flue gas desulfurization control of enterprises, new energy to replace polluting energy, 50% of privately owned vehicles were banned through an odd and even number system, and switching from coal to natural gas for heating. And it is noted that the  $\text{SO}_2$  loadings have been with a short-lived upswing in the early of 11th and 12th five-year plan that may be caused by the government's economy stimulus.

**3.1.2. Seasonal Variations.** A more detailed temporal variation of  $\text{SO}_2$  concentration during 2006–2017 in the BTH region is analyzed. As shown in Figure 7, the  $\text{SO}_2$  seasonal



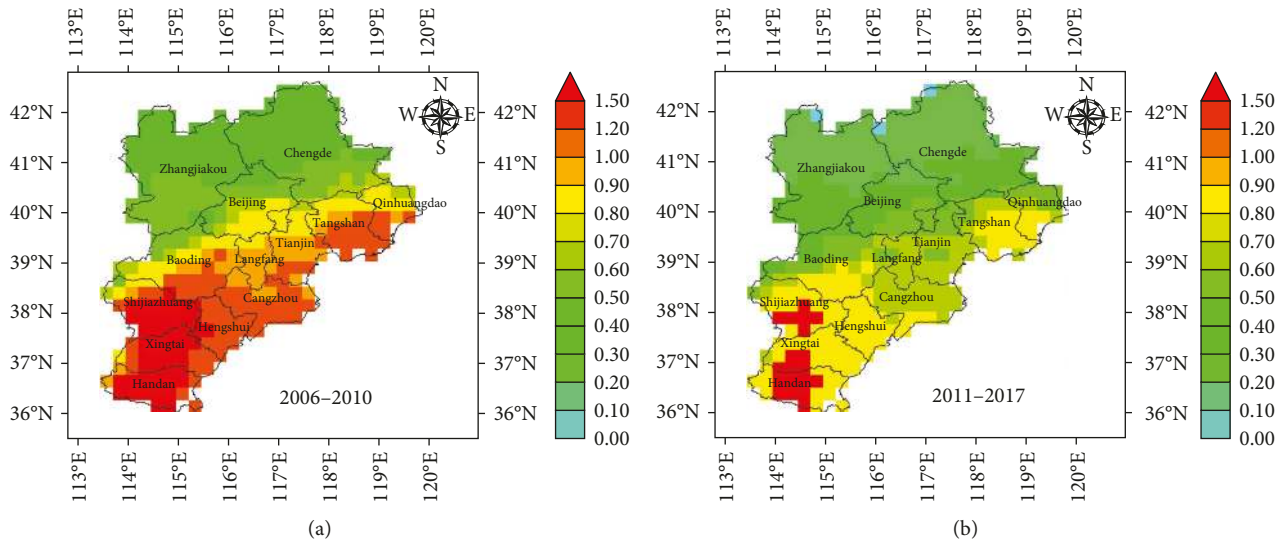


FIGURE 6: Average SO<sub>2</sub> column over the BTH region during 2006–2010 (a) and 2011–2017 (b).

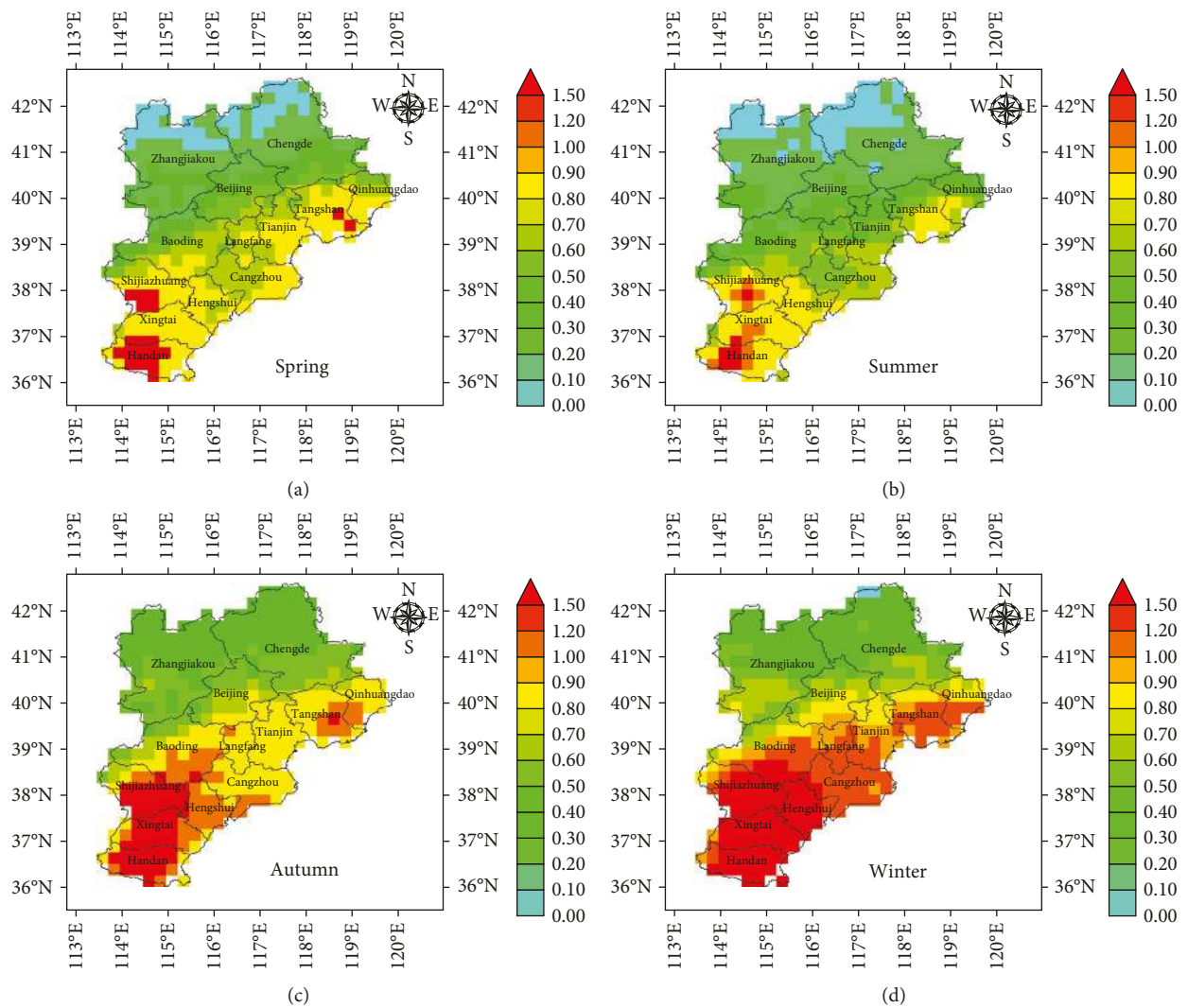


FIGURE 7: Seasonal average SO<sub>2</sub> over the Beijing-Tianjin-Hebei region (in DU), 2006–2017.

mean distribution has an obvious seasonal change sequence as winter (December, January, and February)>autumn (September, October, and November)>spring (March, April, and May)>summer (June, July, and August). The average SO<sub>2</sub> loading of four seasons (spring, summer, autumn, and winter) was 0.59 DU, 0.52 DU, 0.73 DU, and 0.89 DU, respectively. Figure 8 also shows seasonal variation by calculating the monthly SO<sub>2</sub> columns from 2006 to 2017. SO<sub>2</sub> levels are peak in winter and minimum in summer and they are mainly attributed to the difference in pollution diffusion, which is caused by anthropogenic activities and meteorological conditions. Coal heating is a major source accounting for high SO<sub>2</sub> levels in winter. The SO<sub>2</sub> rapid drawdown in 2016 and 2017 represents the fact that coal heating had been replaced by natural gas is successful in reducing sulfur dioxide emissions. In addition, the SO<sub>2</sub> in the PBL has short lifetimes during the warm season, on the short time scale of days to months, and meteorology plays an important role in regional air pollution [6]. The pollutants in the atmosphere have a dilution effect. The meteorological data of 2007, the highest loading over the past twelve years, were chosen as an example to interpret the seasonal differences (Figure 9). In summer, near-surface temperature is higher and air convection is stronger, besides relative humidity and amount of precipitation reaches the annual maximum. All these aforementioned basics can speed up the diffusion of atmospheric pollutants, which have given birth to short lifetimes of SO<sub>2</sub> loading. On the contrary, the temperature, relative humidity, and precipitation in winter go against the transformation from SO<sub>2</sub> to sulfate, making the SO<sub>2</sub> with the longest lifetime in winter [48].

**3.2. Spatial Distribution Pattern.** In Figure 10, the spatial distribution of the average SO<sub>2</sub> column in the Beijing-Tianjin-Hebei region from 2006 to 2017 is presented. As shown in Figure 10, the high SO<sub>2</sub> concentration in BTH is significantly distributed in the southwest and eastern regions.

As for the thirteen cities, multiyear average SO<sub>2</sub> clearly presents the spatial distribution discrepancy. We set up two borderlines with SO<sub>2</sub> column amount (1.0 DU and 0.5 DU) to identify hotspots over BTH (Figure 11). The SO<sub>2</sub> concentrations of Handan, Xingtai, and Shijiazhuang in the southwest of BTH are more than 1.0 DU. Cities with SO<sub>2</sub> concentrations exceeding 0.5 DU include Tangshan, Tianjin, and Qinhuangdao located in the coastal beach areas of Bohai Bay, Hengshui, and Cangzhou adjacent to the Shandong province, as well as Baoding and Langfang around Beijing. The SO<sub>2</sub> loading of Zhangjiakou and Chengde in the north BTH region cities are lower than the other eleven cities less than 0.5 DU.

The characteristic of spatial distribution over BTH can be interpreted from both natural factors and human activities. As shown in Figure 12, the terrain declines semicircularly from the northwest to the southeast over the BTH region due to the mountains and plains landforms. Figure 13 also shows the landscapes in this region, plateaus, mountains, and hills account for 54% of the entire BTH region centering on the area of northwest. Surface pressures gradually decrease from eastern to the northwest over the mountains (Figure 14). The central and southeast plains account for 46% of the region.

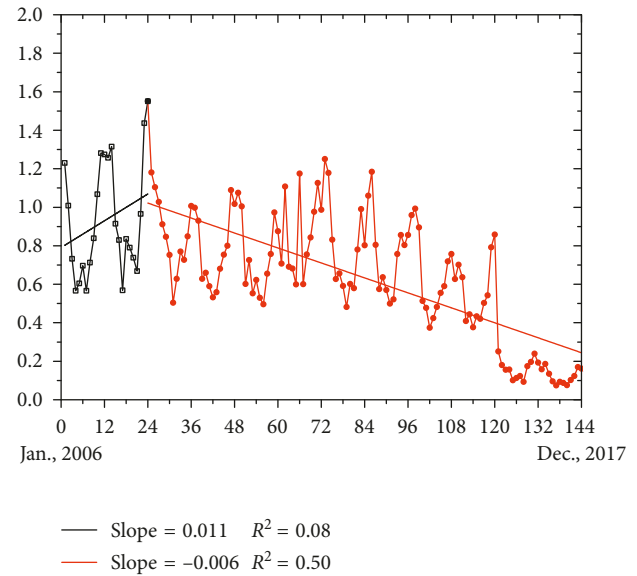


FIGURE 8: Long trend of SO<sub>2</sub> column over the BTH region during two periods, 2006–2007 and 2007–2017.

Forests and grasslands are representative natural ecological landscapes in the region and account for 38% of the study area, and they are mainly distributed in the Yanshan Mountains, the Taihang Mountains, and the northwest edge of the Inner Mongolia Plateau [49]. We also found that relative humidity is different in this region due to the terrain and surface coverage (Figure 9). The whole area is mostly above 30%, especially the northwest is with higher values above 50% in winter, and wind also plays a major part in contributing to the SO<sub>2</sub> spatial distribution. Wind direction and wind speeds determine the pollutant transmission path and diffusion velocity. The southern part of BTH underlies the leeward area which makes the SO<sub>2</sub> difficult to diffusion and dilution, leading to the SO<sub>2</sub> accumulation. However, the area of northern BTH located in the upwind accompanied with high wind speeds in favor of SO<sub>2</sub> diffusion as shown in Figure 14. From the point of human factors, coal, petrification, motor vehicles, and iron and steel industrial emissions are the major source of the BTH region, which has a close relationship with the spatial distribution of population. The spatial pattern of population over BTH exhibits that the southern plain area is more likely to cause human activities variance than the northern region. The southern region is so flat and densely populated that human activities and industrial emissions greatly influence the environment.

Besides natural factors discussed above, anthropogenic factors also take up significant role, contributing to heavy pollution. The BTH region is adjacent to Inner Mongolia, Shanxi, Shandong, and Henan, which is the top five major pollution emission provinces in China (Figure 12), where gathering the most heavily emission sources in China is shown in Figure 3. As shown in Figure 15, we calculate the annual SO<sub>2</sub> columns for each city of the BTH region. Handan, Xingtai, and Shijiazhuang as the emission hotspots will be served for further analysis. At first, the high SO<sub>2</sub> loadings in the southwest of BTH around the province of

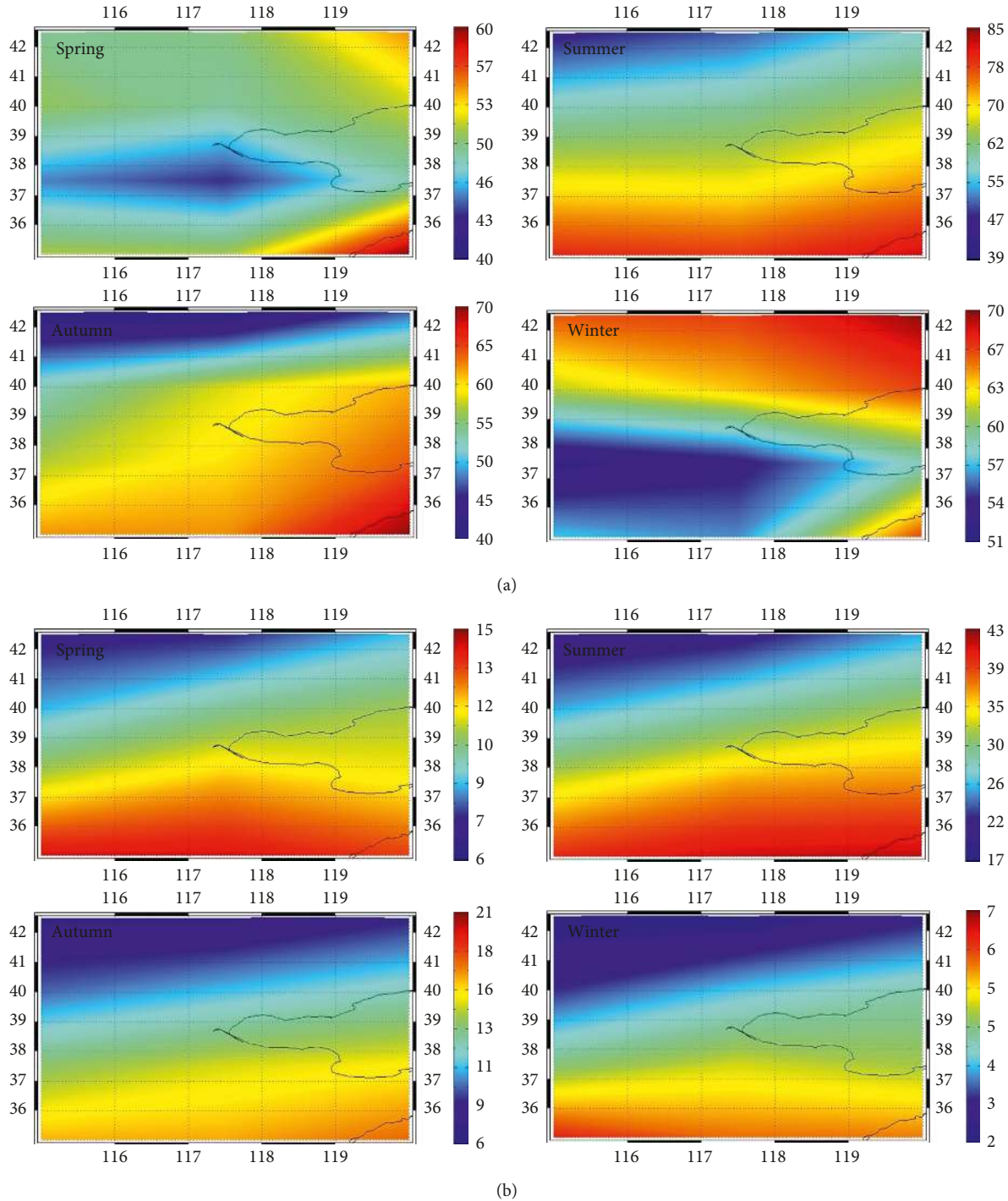
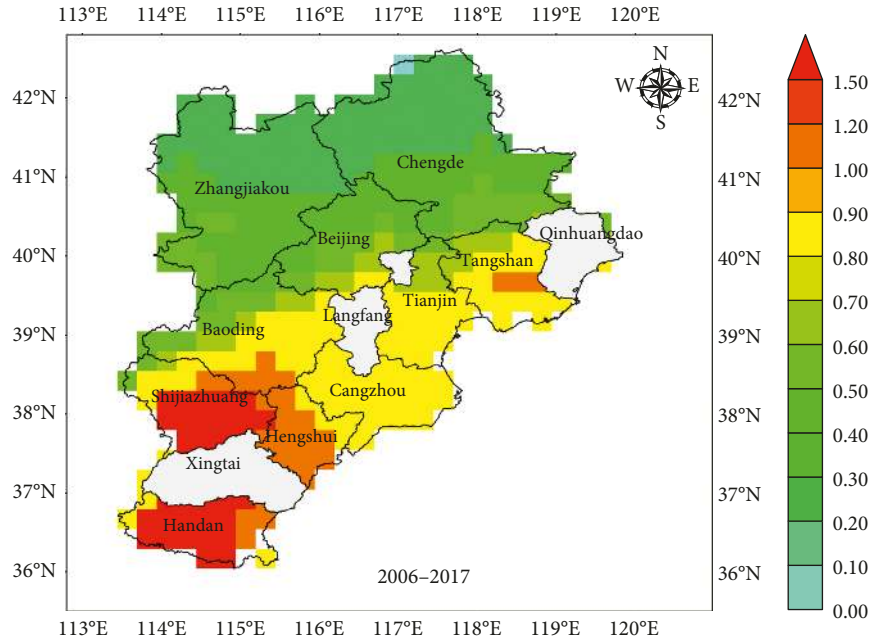
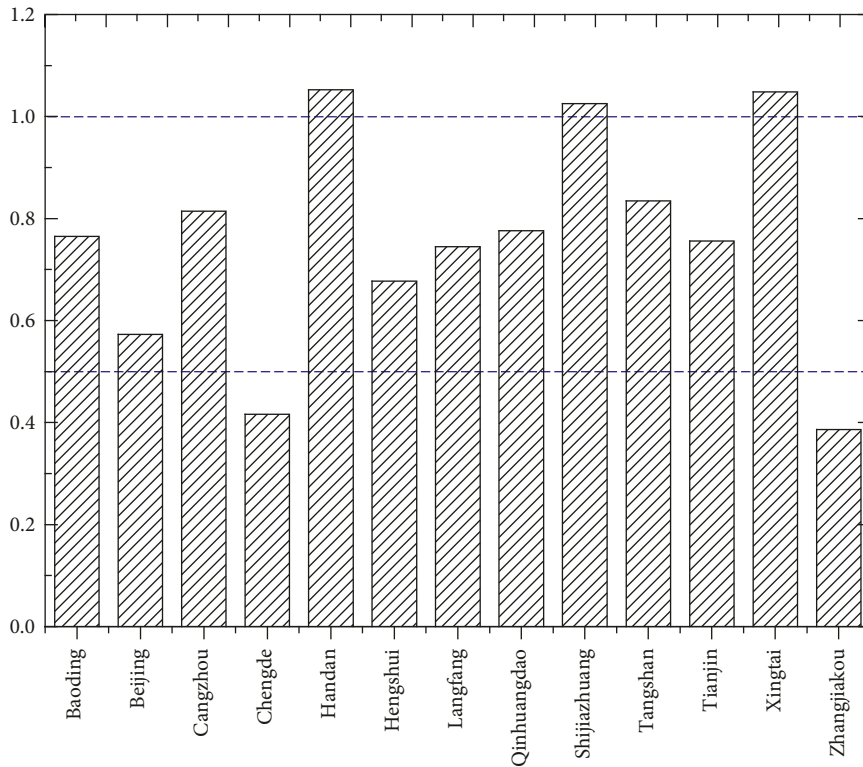


FIGURE 9: Seasonal mean of climatology variables. (a) Relative humidity (%) and (b) precipitable water content ( $\text{kg/m}^2$ ).

Shanxi has nearly a hundred of coal-fired power plants that help contribute to the higher value. Secondly, the BTH region has the largest iron and steel industrial scale in China, among that Beijing, Tianjin, Shijiazhuang, Handan, and Tangshan occupies the majority. Meanwhile, these cities have been the most polluted in BTH region due to unfavourable factors, such as meteorological and geographic conditions and population density. Tangshan, the iron and steel producer of Hebei province, is the second most polluted

city because of its high smoke  $\text{SO}_2$  emission. Although population and enterprises of Beijing are high, the highest green coverage rate and strict pollution control measures make the pollution level relatively low in the BTH region. Zhangjiakou and Chengde had a low  $\text{SO}_2$  column with the least amount of population density, industrial enterprises as well as the terrain advantage. The amplitude of each urban curves variation is able to reveal the degree of being influenced by natural and anthropogenic sources.



FIGURE 10: Multiyear average  $\text{SO}_2$  spatial distribution map over the BTH region.FIGURE 11: Average  $\text{SO}_2$  column (in DU, twelve years) of thirteen cities in the BTH region.

**3.3. Typical Pollution Control Cases.** As analyzed in Sections 3.1 and 3.2, there is an overall large decreasing trend of  $\text{SO}_2$  emission since 2011. The increasing/decreasing trend of  $\text{SO}_2$  in this period has been discussed with decadal, seasonal, and district variability. The results suggest that long-term variations are attributed to stricter emission reduction. In particular, three typical episodes (the Olympic Games in

2008, the Asia-Pacific Economic Cooperation (APEC) in 2014, and Military Parade in 2015) have been taken place in Beijing during 2006–2017. A series of strengthened emission reduction measures have played an important role in preventing and controlling air pollution, which significantly improved the air quality in Beijing and neighboring regions [50–54]. Therefore, we evaluate the variation (Figure 8) by

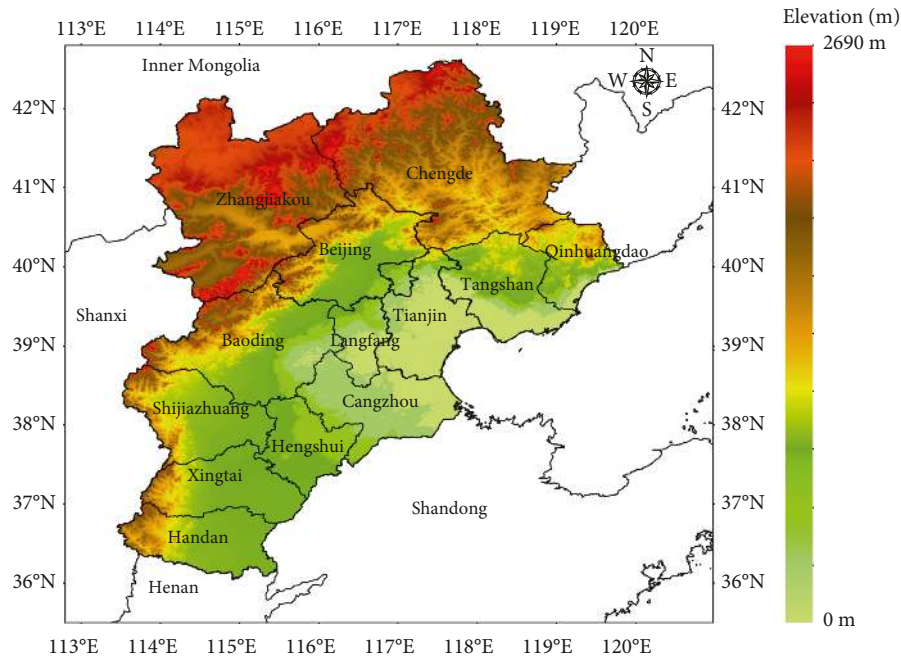


FIGURE 12: Topography of the Beijing-Tianjin-Hebei (BTH) region.

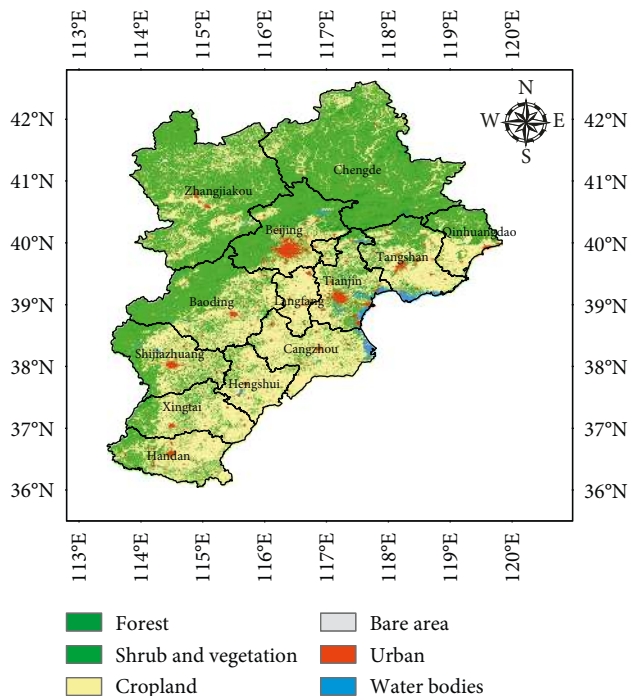


FIGURE 13: The main landscape type over the Beijing-Tianjin-Hebei (BTH) region.

tracking the changes of  $\text{SO}_2$  to reveal the effective operations driven by environmental policy and measures. The 29th Olympic Games were held in Beijing, started on 8 August 2008, the 2014 Asia-Pacific Economic Cooperation (APEC) Economic Leaders' Meeting was held on November 10 and 11 in Beijing, and China Military Parade was held on 3 September 2015. Prior to the events, emission reduction

measures were began to conduct. Monthly,  $\text{SO}_2$  column concentration of other years from 2006 to 2017 corresponding to these periods have been compared with the basis of 2006.

As shown in Figure 16, the  $\text{SO}_2$  average concentration for the period of Olympic Games decreased significantly to 14.92% and 7.76% compared to the neighboring years; the average  $\text{SO}_2$  concentration in the APEC conference was significantly lower than that of the same periods in past ten years, and it declined 28.57% compared to the average of November in other years between 2006 and 2015; and the  $\text{SO}_2$  concentration in September of the 2015 Military Parade, with 27.43% decline, reached the lowest value compared to ten years before. Standard deviations can reflect that more clearly. Besides, the standard deviations verify the previous analysis of seasonal characteristic and brief ascent in 2011.

During the three events, air pollution control policies have been reinforced. To achieve the goal of "green Olympic Games" [55], China has released a series of air pollution control policies to improve air quality. The government has implemented a series of long-term pollution reduction measures, such as coal-fired power plant in Beijing to install the desulfurization equipment, part of closure of small power plants in this area near Beijing during the Olympic Games, and about 94% of the small coal-fired boilers to use clean energy transformation. The government also implemented some short-term strategies; for example, from July 1st to September 20th of 2008, the vehicles with exhaust emissions that failed to meet the European No. 1 standard were all-day forbidden on the roads; from July 20th to September 20th, the odd/even license plate number rule was applied on personal vehicles in Beijing [12]; power generation facilities were run only 30% of the equipment to stop all construction activities; some heavy-polluting factories were closed during the Olympic Games; and some heavily polluting

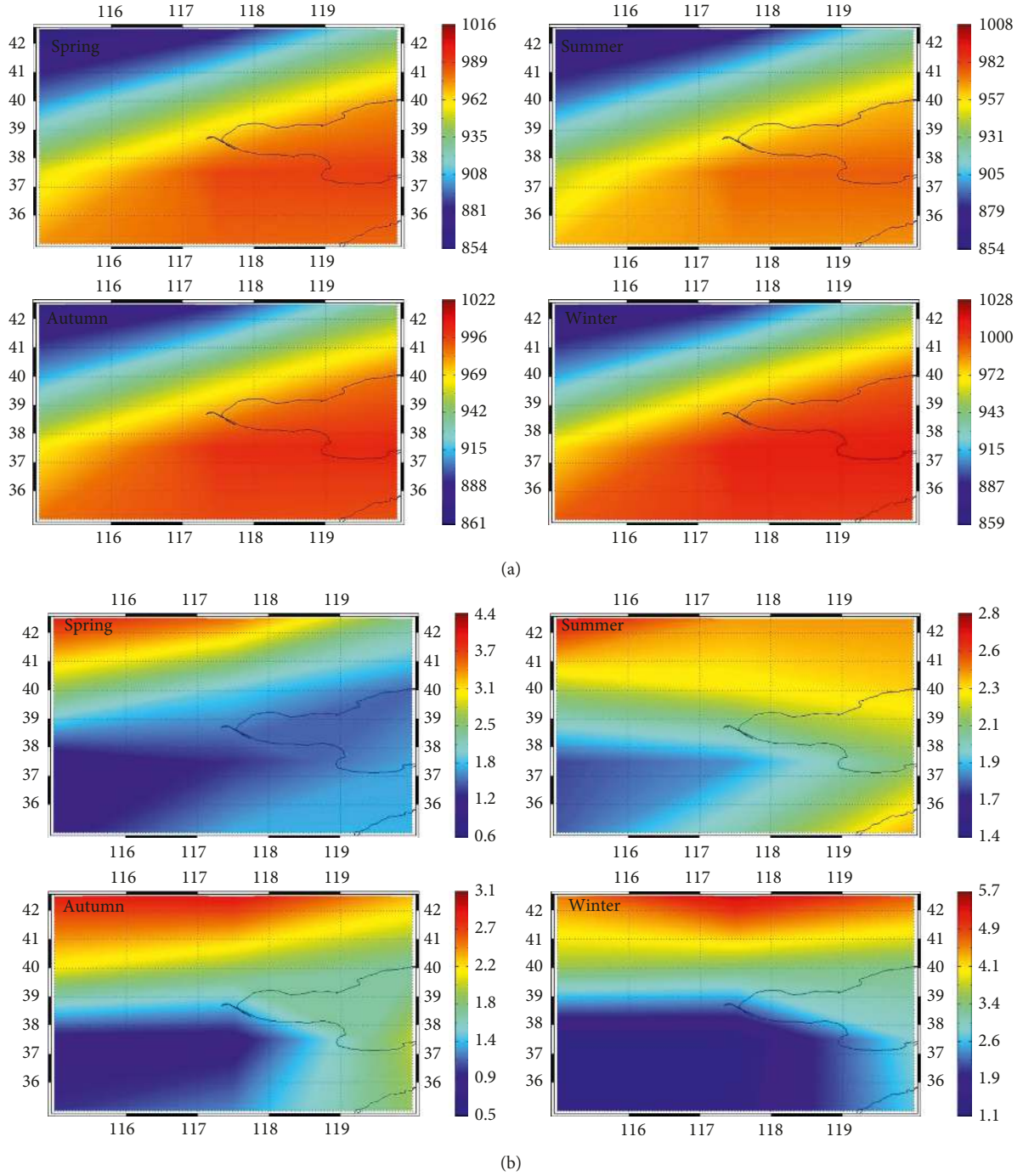


FIGURE 14: Seasonal mean of climatology variables. (a) Surface pressure (millibars) and (b) wind speed (m/s).

companies around Beijing city were closed [29, 31]. During the APEC meeting and the Military Parade, the government also implemented a series of measures to ensure the safety and environmental protection measures, and these measures are similar even more and stricter than the 2008 Olympic Games, as with Beijing, the surrounding six provinces also have taken similar measures [27, 56]. During the period from August 20th to September 3rd of 2015, Beijing adopted to strengthen urban transportation management to strictly limit the motor vehicle population [57].

Relevant conclusion comes out that any air pollution activities by human beings in the entire BTH region should be controlled with the most rigorous management. Beijing as China's political and administrative center has strict pollution control measures and high execution efficiency. Meanwhile, the environment policies to a certain extent affect the surrounding cities of Beijing. We focused on several affairs, such as the 2008 Olympic Games, 2014 APEC (Asia-Pacific Economic Cooperation), and 2015 Victory Day Military Parade, by means of analyzing the concentration of  $\text{SO}_2$  during the

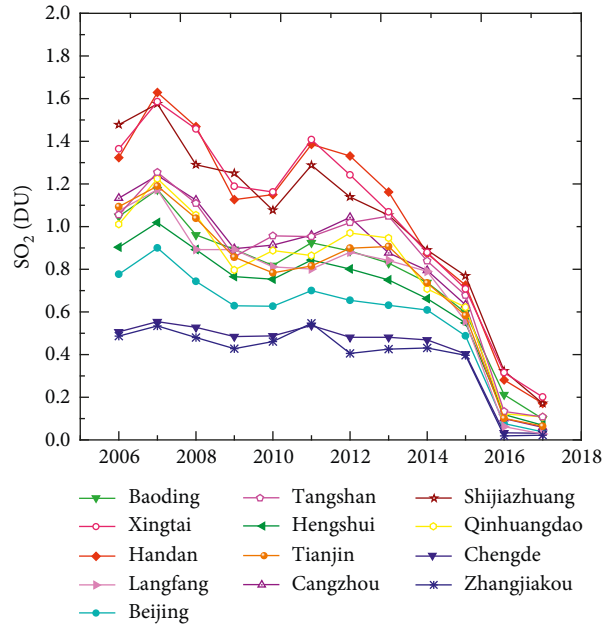


FIGURE 15: Annual mean curve of  $\text{SO}_2$  column concentration of each city in the BTH region, 2006–2017.

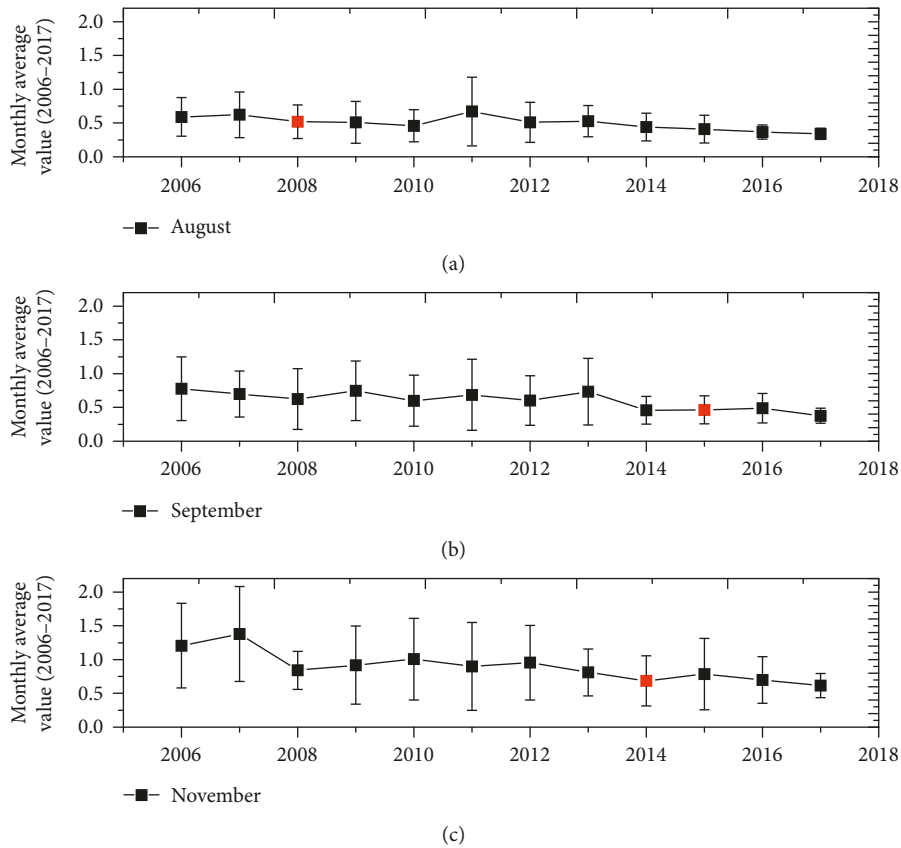


FIGURE 16: Monthly average  $\text{SO}_2$  of August (a), September (b), and November (c) from 2006 to 2017. The black solid squares show relative changes based on 2006. The error bars express standard deviation. The red solid squares represent the months when events occur.

events to confirm the effectiveness of environmental management measures. The relative changes clearly demonstrate that these measures were effective in reducing  $\text{SO}_2$  concentration during the periods of those affairs taken place.

#### 4. Conclusions

In this study, the past 12 years (2006–2017), OMI observations have yielded profound insights into the spatial distribution



and temporal trends in SO<sub>2</sub> emission over the Beijing-Tianjin-Hebei region. The SO<sub>2</sub> loading distribution has close correlation with their emission sources. Spatiotemporal variation characteristics over BTH can more clearly reflect the natural and anthropogenic emission sources, to provide references to air pollution prevention and control. The main conclusions are as follows:

- (1) The temporal changes (2006–2017) over the BTH region exhibit the upward and downward trend consistent with the national trend in China. According to the dipping and heaving, we find that the gridded SO<sub>2</sub> data can be divided into two phases: the first (2006–2010) and second (2011–2017) period, to observe changes in SO<sub>2</sub> loadings presenting the Chinese government actions and policies and accomplishments in addressing air pollution. The SO<sub>2</sub> loadings have drastically decreased by more than 30% from the 2006–2010 period to the 2011–2017 period. SO<sub>2</sub> peaked in 2007 and the secondary peak was in 2011, to a certain extent, referring to the economic policy stimulus in the early of each FYP. Meanwhile, OMI observations show generally good agreement with independent SO<sub>2</sub> emission.
- (2) The annual cycles of SO<sub>2</sub> show a pronounced seasonal pattern, with the highest values occurring in winter and the lowest values in summer. This seasonal variation can be explained mainly by the seasonality of emission strengths, lifetimes of these pollutants, and meteorological factors.
- (3) Spatial distribution of BTH is also characterized, which is interesting to find that progressive changes from the northern to the southern regions are associated with the terrain and surface coverage, besides industrial pattern and population distribution. In the cities of BTH, we found that rapid SO<sub>2</sub> reductions generally correlate well with sharp reductions in industrial activity.
- (4) China made great progress in pollution control with implementation of a series of major policies. The concentration of SO<sub>2</sub> during 2008 Olympic Games, 2014 APEC, and 2015 Military Parade have been compared to identical months in other years, and the result shows that concentration of SO<sub>2</sub> column was relatively low in these episodes because of reinforced emission controls.

These findings demonstrate that SO<sub>2</sub> concentration over BTH do not follow simple linear trends, but instead reflect a repercussion of environmental measures and political economic activities. In terms of temporal changes, the decreasing trend has been observed since 2011, mainly due to the government efforts to restrain emissions from the power and industrial sectors. On the other hand, spatial characteristics are regarding with natural and anthropogenic factors. One of the important goals in this work is to evaluate the effectiveness of a series of policy to control the pollution problems, and three typical time quantum status reflects that the national environmental pollution control measures have taken an evident effect. These findings can provide a basis for

the development of environmental management measures during the Winter Olympics in 2022, also for the national environmental pollution prevention and control as a reference. The results clearly illustrate effectiveness of central governmental policies regarding emission mitigation of SO<sub>2</sub> and aid in important policy implications for the future reduction action plans to provide better air quality of China.

## Data Availability

The OMI SO<sub>2</sub> data are downloaded from <http://giovanni.gsfc.nasa.gov/giovanni/>. The meteorological data are from <https://www.esrl.noaa.gov/psd/>. The SO<sub>2</sub> emission data have been publicly released from <http://www.stats.gov.cn/tjsj/>. The data used to support the findings of this study are included within the article.

## Conflicts of Interest

The authors declare that they have no conflicts of interest.

## Acknowledgments

This study was supported by the National Natural Science Foundation of China (Grant no. 41501404) and Natural Science Foundation of Hebei Province under Project no. F2017203220.

## References

- [1] R. Wayne, *Chemistry of Atmospheres*, Oxford Science Publications, Oxford, UK, 1991.
- [2] J. H. Seinfeld and S. N. Pandis, *Atmospheric Chemistry and Physics: From Air Pollution to Climate Change*, John Wiley & Sons, Hoboken, NJ, USA, 2nd edition, 2006.
- [3] M. Chin, R. B. Rood, S. J. Lin et al., “Atmospheric sulfur cycle simulated in the global model GOCART: model description and global properties,” *Journal of Geophysical Research: Atmospheres*, vol. 105, no. D20, pp. 24671–24687, 2000.
- [4] B. Denby, I. Sundvor, M. Cassiani et al., “Spatial mapping of ozone and SO<sub>2</sub> trends in Europe,” *Science of the Total Environment*, vol. 408, no. 20, pp. 4795–4806, 2010.
- [5] V. E. Fioletov, C. A. McLinden, N. Krotkov, M. D. Moran, and K. Yang, “Estimation of SO<sub>2</sub> emissions using OMI retrievals,” *Geophysical Research Letters*, vol. 38, no. 21, 2011.
- [6] C. Lee, R. V. Martin, A. Van Donkelaar et al., “SO<sub>2</sub> emissions and lifetimes: estimates from inverse modeling using in situ and global, space-based (SCIAMACHY and OMI) observations,” *Journal of Geophysical Research Atmospheres*, vol. 116, no. D6, 2011.
- [7] Z. Klimont, S. J. Smith, and J. Cofala, “The last decade of global anthropogenic sulfur dioxide: 2000–2011 emissions,” *Environmental Research Letters*, vol. 8, no. 1, pp. 1880–1885, 2013.
- [8] J. L. Hand, B. A. Schichtel, W. C. Malm et al., “Particulate sulfate ion concentration and SO<sub>2</sub> emission trends in the United States from the early 1990s through 2010,” *Atmospheric Chemistry and Physics*, vol. 12, no. 21, pp. 10353–10365, 2012.
- [9] N. Theys, I. De Smedt, J. Gent et al., “Sulfur dioxide vertical column DOAS retrievals from the Ozone Monitoring Instrument: global observations and comparison to ground-based and satellite data,” *Journal of Geophysical Research: Atmospheres*, vol. 120, no. 6, pp. 2470–2491, 2015.
- [10] H. He, K. Y. Vinnikov, C. Li et al., “Response of SO<sub>2</sub> and particulate air pollution to local and regional emission

- controls: a case study in Maryland,” *Earth’s Future*, vol. 4, no. 4, pp. 94–109, 2016.
- [11] N. A. Krotkov, B. McClure, R. R. Dickerson et al., “Validation of SO<sub>2</sub> retrievals from the Ozone Monitoring Instrument over NE China,” *Journal of Geophysical Research: Atmospheres*, vol. 113, no. D16, pp. 16–40, 2008.
  - [12] C. Gao, H. Yin, N. Ai et al., “Historical analysis of SO<sub>2</sub> pollution control policies in China,” *Environmental Management*, vol. 43, no. 3, pp. 447–457, 2009.
  - [13] H. He, C. Li, C. P. Loughner et al., “SO<sub>2</sub> over central China: measurements, numerical simulations and the tropospheric sulfur budget,” *Journal of Geophysical Research: Atmospheres*, vol. 117, no. D16, pp. 812–819, 2012.
  - [14] C. Li, Q. Zhang, N. A. Krotkov et al., “Recent large reduction in sulfur dioxide emissions from Chinese power plants observed by the Ozone Monitoring Instrument,” *Geophysical Research Letters*, vol. 37, no. 8, pp. 292–305, 2010.
  - [15] J. Lin, C. P. Nielsen, Y. Zhao et al., “Recent changes in particulate air pollution over China observed from space and the ground: effectiveness of emission control,” *Environmental Science & Technology*, vol. 44, no. 20, pp. 7771–7776, 2010.
  - [16] Z. Lu, D. G. Streets, Q. Zhang et al., “Sulfur dioxide emissions in China and sulfur trends in East Asia since 2000,” *Atmospheric Chemistry and Physics*, vol. 10, no. 4, pp. 6311–6331, 2010.
  - [17] W. Zhang, H. Xu, F. Zheng et al., “Classifying aerosols based on fuzzy clustering and their optical and microphysical properties study in Beijing, China,” *Advances in Meteorology*, vol. 2017, Article ID 4197652, 18 pages, 2017.
  - [18] A. Krueger, “Sighting of El chichón sulfur dioxide clouds with the nimbus 7 total ozone mapping spectrometer,” *Science*, vol. 220, no. 4604, pp. 1377–1379, 1983.
  - [19] M. Eisinger and J. P. Burrows, “Tropospheric sulfur dioxide observed by the ERS-2 GOME instrument,” *Geophysical Research Letters*, vol. 25, no. 22, pp. 4177–4180, 1998.
  - [20] J. P. Burrows, M. Weber, M. Buchwitz et al., “The global ozone monitoring experiment (GOME): mission concept and first scientific results,” *Journal of Atmospheric Sciences*, vol. 56, no. 2, pp. 151–175, 1999.
  - [21] M. F. Khokhar, U. Platt, and T. Wagner, “Satellite observations of atmospheric SO<sub>2</sub> from volcanic eruptions,” in *Proceedings of the 35th COSPAR Scientific Assembly*, Paris, France, June 2004.
  - [22] H. Bovensmann, J. P. Burrows, M. Buchwitz et al., “SCIAMACHY: mission objectives and measurement modes,” *Journal of Atmospheric Sciences*, vol. 56, no. 2, pp. 127–150, 1999.
  - [23] J. Callies, E. Corpaccioli, M. Eisinger, A. Hahne, and A. Lefebvre, “GOME-2-Metop’s second-generation sensor for operational ozone monitoring,” *ESA Bulletin*, vol. 102, pp. 28–36, 2000.
  - [24] P. F. Levelt, G. H. J. V. D. Oord, M. R. Dobber et al., “The ozone monitoring instrument,” *IEEE Transactions on Geoscience and Remote Sensing*, vol. 44, no. 5, pp. 1093–1101, 2006.
  - [25] W. Zhang, X. Gu, H. Xu, T. Yu, and F. Zheng, “Assessment of OMI near-UV aerosol optical depth over Central and East Asia,” *Journal of Geophysical Research: Atmospheres*, vol. 121, no. 1, pp. 382–398, 2016.
  - [26] Q. Zhang, D. G. Streets, and K. He, “Satellite observations of recent power plant construction in Inner Mongolia, China,” *Geophysical Research Letters*, vol. 36, no. 15, pp. 1–5, 2009.
  - [27] S. Wang, Q. Zhang, R. V. Martin et al., “Satellite measurements oversee China’s sulfur dioxide emission reductions from coal-fired power plants,” *Environmental Research Letters*, vol. 10, no. 11, article 114015, 2015.
  - [28] J. Jie, Z. Yong, G. Jay, and J. Jianjun, “Monitoring of SO<sub>2</sub> column concentration change over China from Aura OMI data,” *International Journal of Remote Sensing*, vol. 33, no. 6, pp. 1934–1942, 2012.
  - [29] J. C. Witte, M. R. Schoeberl, A. R. Douglass et al., “Satellite observations of changes in air quality during the 2008 Beijing Olympics and Paralympics,” *Geophysical Research Letters*, vol. 36, no. 17, pp. 37–44, 2009.
  - [30] Z. Leishi, L. C. Sheng, Z. Ruiqin, and C. Liangfu, “Spatial and temporal evaluation of long term trend (2005–2014) of OMI retrieved NO<sub>2</sub> and SO<sub>2</sub> concentrations in Henan Province, China,” *Atmospheric Environment*, vol. 154, pp. 151–166, 2016.
  - [31] L. T. Wang, C. Jang, Y. Zhang et al., “Assessment of air quality benefits from national air pollution control policies in China. Part I: background, emission scenarios and evaluation of meteorological predictions,” *Atmospheric Environment*, vol. 44, no. 28, pp. 3449–3457, 2010.
  - [32] L. Feng and W. Liao, “Legislation, plans, and policies for prevention and control of air pollution in China: achievements, challenges, and improvements,” *Journal of Cleaner Production*, vol. 112, pp. 1549–1558, 2017.
  - [33] C. Li, C. McLinden, V. Fioletov et al., “India is overtaking China as the world’s largest emitter of anthropogenic sulfur dioxide,” *Scientific Reports*, vol. 7, no. 1, 2017.
  - [34] N. A. Krotkov, C. A. McLinden, C. Li et al., “Aura OMI observations of regional SO<sub>2</sub> and NO<sub>2</sub> pollution changes from 2005 to 2014,” *Atmospheric Chemistry and Physics*, vol. 15, no. 19, pp. 26555–26607, 2015.
  - [35] S. P. Ahmad, P. F. Levelt, P. K. Bhartia, E. Hilsenrath, G. W. Leppelmeier, and J. E. Johnson, “Atmospheric products from the ozone monitoring instrument (OMI),” *Earth Observing Systems VIII*, vol. 5151, pp. 619–630, 2003.
  - [36] NASA Goddard Earth Sciences, “Aura OMI sulphur dioxide data product-OMSO<sub>2</sub>,” April 2016, [http://disc.sci.gsfc.nasa.gov/Aura/data-holdings/OMI/omso2\\_v003.shtml](http://disc.sci.gsfc.nasa.gov/Aura/data-holdings/OMI/omso2_v003.shtml).
  - [37] A. I. Prados, G. Leptoukh, C. Lynnes et al., “Access, visualization, and interoperability of air quality remote sensing data sets via the Giovanni online tool,” *IEEE Journal of Selected Topics in Applied Earth Observations and Remote Sensing*, vol. 3, no. 3, pp. 359–370, 2010.
  - [38] C. Mallik and S. Lal, “Seasonal characteristics of SO<sub>2</sub>, NO<sub>2</sub>, and CO emissions in and around the Indo-Gangetic Plain,” *Environmental Monitoring and Assessment*, vol. 186, no. 2, pp. 1295–1310, 2014.
  - [39] N. A. Krotkov, S. A. Carn, A. J. Krueger et al., “Band residual difference algorithm for retrieval of SO/sub 2/ from the aura ozone monitoring instrument (OMI),” *IEEE Transactions on Geoscience and Remote Sensing*, vol. 44, no. 5, pp. 1259–1266, 2006.
  - [40] C. Li, J. Joiner, N. A. Krotkov et al., “A fast and sensitive new satellite SO<sub>2</sub> retrieval algorithm based on principal component analysis: Application to the ozone monitoring instrument,” *Geophysical Research Letters*, vol. 40, no. 23, pp. 6314–6318, 2013.
  - [41] C. Li, N. A. Krotkov, S. Carn et al., “New-generation NASA Aura Ozone Monitoring Instrument (OMI) volcanic SO<sub>2</sub> dataset: algorithm description, initial results, and continuation with the Suomi-NPP Ozone Mapping and Profiler Suite (OMPS),” *Atmospheric Measurement Techniques Discussions*, vol. 10, pp. 1–27, 2017.
  - [42] H. H. Yan, X. J. Li, X. Y. Zhang et al., “Comparison and validation of band residual difference algorithm and principal component analysis algorithm for retrievals of atmospheric SO<sub>2</sub> columns from satellite observations,” *Acta Physica Sinica*, vol. 65, no. 8, 2016.
  - [43] NBS, *China Energy Statistical Yearbook*, National Bureau of Statistics of China, China Statistics Press, Beijing, China, 2016.

- [44] V. E. Fioletov, C. A. McLinden, N. Krotkov et al., “Lifetimes and emissions of SO<sub>2</sub> from point sources estimated from OMI,” *Geophysical Research Letters*, vol. 42, no. 6, pp. 1969–1976, 2015.
- [45] V. E. Fioletov, C. A. McLinden, N. Krotkov et al., “A global catalogue of large SO<sub>2</sub> sources and emissions derived from the Ozone Monitoring Instrument,” *Atmospheric Chemistry and Physics*, vol. 16, no. 18, pp. 11497–11519, 2016.
- [46] N. A. Krotkov, C. A. McLinden, C. Li et al., “Aura OMI observations of regional SO<sub>2</sub> and NO<sub>2</sub> pollution changes from 2005 to 2015,” *Atmospheric Chemistry and Physics*, vol. 16, no. 7, pp. 4605–4629, 2016.
- [47] X. Hualin, H. Yafen, and X. Xue, “Region using big data exploring the factors influencing ecological land change for China’s Beijing-Tianjin-Hebei,” *Journal of Cleaner Production*, vol. 142, no. 2, pp. 677–687, 2017.
- [48] C. Calkins, C. Ge, J. Wang et al., “Effects of meteorological conditions on sulfur dioxide air pollution in the North China plain during winters of 2006–2015,” *Atmospheric Environment*, vol. 147, pp. 296–309, 2016.
- [49] P. Li, Y. Lv, C. Zhang et al., “Analysis and planning of ecological networks based on kernel density estimations for the Beijing-Tianjin-Hebei region in Northern China,” *Sustainability*, vol. 8, no. 11, p. 1094, 2016.
- [50] Y. Wang, J. Hao, M. B. McElroy et al., “Ozone air quality during the 2008 Beijing Olympics-effectiveness of emission restrictions,” *Atmospheric Chemistry and Physics Discussions*, vol. 9, no. 2, pp. 9927–9959, 2009.
- [51] Y. Gao and M. Zhang, “Sensitivity analysis of surface ozone to emission controls in Beijing and its neighboring area during the 2008 Olympic Games,” *Journal of Environmental Sciences*, vol. 24, no. 1, pp. 50–61, 2012.
- [52] Li Sheng a, K. Lu, X. Ma et al., “The air quality of Beijing-Tianjin-Hebei regions around the Asia-Pacific Economic Cooperation (APEC) meetings,” *Atmospheric Pollution Research*, vol. 6, no. 6, pp. 1066–1072, 2015.
- [53] G. Wang, S. Cheng, W. Wei et al., “Characteristics and emission-reduction measures evaluation of PM 2.5 during the two major events: APEC and Parade,” *Science of the Total Environment*, vol. 595, pp. 81–92, 2017.
- [54] Y. Zheng, H. Che, T. Zhao, X. Xia, K. Gui, and L. An, “Aerosol optical properties over Beijing during the World Athletics Championships and Victory Day Military Parade in August and September 2015,” *Atmosphere*, vol. 7, no. 3, pp. 47–62, 2016.
- [55] Beijing Organizing Committee for the Games of the XXIX Olympic Games (BOCOG), *Green Olympics in Beijing*, BOCOG, Beijing, China, 2005.
- [56] F. Li, Z. Song, and W. Liu, “China’s energy consumption under the global economic crisis: decomposition and sectoral analysis,” *Energy Policy*, vol. 64, pp. 193–202, 2014.
- [57] Beijing Municipal Environmental Protection Bureau, “Air pollution prevention and control action plan,” 2014, [http://www.gov.cn/zwjk/2013-09/12/content\\_2486773.htm](http://www.gov.cn/zwjk/2013-09/12/content_2486773.htm).



